IJE TRANSACTIONS B: Applications Vol. 37, No. 05, (May 2024) 860-875

International Journal of Engineering

Journal Homepage: www.ije.ir

Optimizing Heat Transfer in Microchannel Heat Sinks: A Numerical Investigation with Nanofluids and Modified Geometries

F. Nasiri Khamesloo, D. Domiri Ganji*

Department of Mechanical Engineering, Babol Noshirvani University of Technology, Babol, Iran

P A P E R I N F O

Paper history:
Received 26 September 2023
Received in revised form 26 November 2023
Accepted 27 November 2023

Keywords:
Numerical Study
Microchannel Heat Sink
Fractal
Nanofluid
Geometry Change

A B S T R A C T

The utilization of microchannel heat sinks stands as one of the most reliable solutions for dissipating heat generated in electronic chips. In this numerical study, a fractal microchannel heat sink employing three nanofluids Cu-water, Al_2O_3-water, and TiO_2-water with variable volume fractions of 2 and 4 percent as the cooling fluid within the microchannels was investigated. The fluid flow inside the microchannels was analyzed from both hydrodynamic and thermal perspectives. The parameters such as pump power, Nusselt number, and performance evaluation criterion (PEC) were studied. Results demonstrate that heat transfer increases with an increase in the flow rate and volume fraction of nanoparticles. The maximum temperature reduction for the Cu-water nanofluid at an inlet flow rate of 200 ml/min and a volume fraction of 4% is 2.41%, the highest among the investigated nanofluids. However, this nanofluid also exhibits the highest pressure drop, reaching 25% at a 4% volume fraction. The PEC number analysis reveals an overall performance increase for all three microchannels. The Cu-water nanofluid exhibits the best comprehensive performance, providing an 8% overall enhancement, followed by Al_2O_3-water and TiO_2-water nanofluids, which increase the system performance by 5% and 4%, respectively. Furthermore, the study introduced fins and cavities to the microchannel branches to enhance heat transfer and overall performance. Results indicate an increase in heat transfer for both modified geometries. The microchannel with fins exhibits a 3.5% lower maximum temperature compared to the original geometry at an inlet flow rate of 200 ml/min, while the microchannel with cavities showed a 1% reduction. However, the microchannel with fins experiences a 400% higher pressure drop than the initial geometry, while the microchannel with cavities has a 4% increase. PEC number analysis demonstrated that the microchannel with cavities improves system performance by 8%, whereas the microchannel with fins reduced system performance by 4%.

doi: *10.5829/ije.2024.37.05b.05*

Graphical Abstract

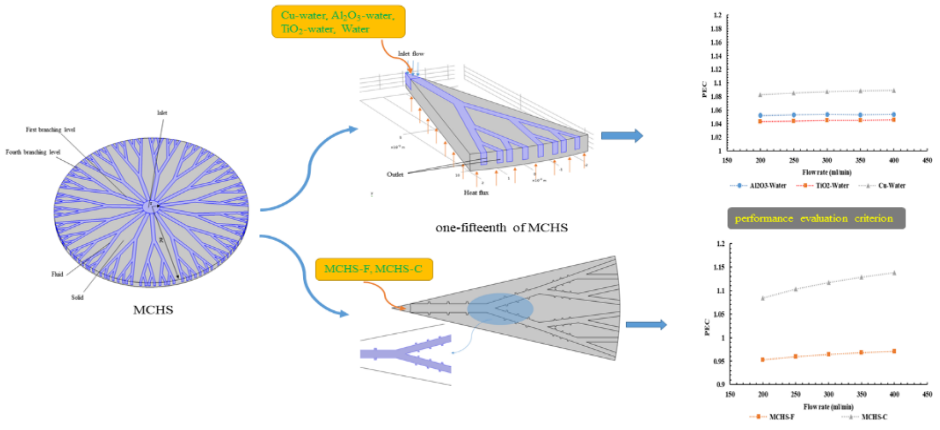

*Corresponding Author Email: mirgang@nit.ac.ir (D. Domiri Ganji)

Please cite this article as: Nasiri Khamesloo F, Domiri Ganji D. Optimizing Heat Transfer in Microchannel Heat Sinks: A Numerical Investigation with Nanofluids and Modified Geometries. International Journal of Engineering, Transactions B: Applications. 2024;37(05):860-75.

Highlights

- Design of a Fractal Microchannel Heat Sink for Numerical Investigation
- Utilization of Three Different Nanofluids for Cooling the Heat Sink and Their Hydraulic and Thermal Comparison
- Cu-Water Nanofluid Demonstrates the Best Overall Performance
- Creation of Fins and Cavities in the Microchannel
- Improved Performance of the Microchannel with Cavities in Terms of Overall Performance

NOMENCLATURE

R	radius of the heat sink (mm)	f	fluid
r	inlet radius (mm)	nf	nanofluid
i	branching level	W_{pump}	pumping power (mW)
u_m	average velocity (m/s)	q_v	flow rate ($m^3 \cdot s^{-1}$)
D_h	hydraulic diameter (mm)	q	Heat flux ($W \cdot m^{-2}$)
c_p	specific heat capacity (J/(kg K))	$Nu_{m.i}$	Nusselt number
T_f	temperature of fluid (K)	**Greek Symbols**	
T_s	temperature of the solid (K)	ρ_f	density of fluid (kg/m^3)
k_f	thermal conductivity of fluid (W/(m K))	μ_f	dynamic viscosity of fluid (N•s/m2)
k_s	thermal conductivity of solid (W/(m K))	φ	volume fraction

1. INTRODUCTION

Since the advent of the first digital electronic devices in the 1940s, efficient heat dissipation has been pivotal in ensuring the performance of subsequent generations of these devices. According to a survey conducted by a multinational corporation, the annual cost of cooling residential computer and telecommunications equipment stands for $4.1 billion. Projections suggest that this expenditure is expected to escalate to $4.8 billion in the foreseeable future. This study underscores the imperative to transcend conventional cooling systems and adopt innovative approaches (1). Heat sinks serve as heat exchangers in electronic devices, managing and dissipating the heat generated by electronic or mechanical chips. Functioning as a thermal management solution, a heat sink absorbs and disperses heat into the surrounding fluid, thereby preventing the temperature of the electronic component from reaching damaging levels. The significance of a heat sink becomes more pronounced when temperature-sensitive components are integrated into the circuit or device. With the ongoing trend of electronic component miniaturization and the associated increase in device temperatures, various methods have been developed to address heat dissipation, including fluid jet impingement, sprays, heat pipes, piezoelectric droplets, and more. Among these techniques, microchannel heat sinks emerge as the most pragmatic choice, boasting advantageous features such as lightweight design, compactness, and a high heat transfer rate to volume ratio (2). Microchannel heat sinks find applications in industries with high heat flux, including oil and gas, steel and metallurgical, energy production and the power electronics industries. They are used for cooling various components such as heat exchangers, piping systems, refinery equipment, steel components, metal smelting furnaces, distillation devices, turbines, generators, power converters, and transistors. These heat sinks are also employed in thermal power plants, photovoltaic concentrator systems, and other high heat flux power plants to cool heat-generating components and systems.

In 1981, Tuckerman and Pease (3) designed the first microchannel heat sink and laid the groundwork for research and development in this field. Weisberg et al. (4) further investigated microchannel heatsinks for cooling electronic chips. They analyzed microchannel heat exchangers using numerical methods and considered dual heat transfer, which involves determining simultaneous temperature fields in solid and fluid media. Additionally, they presented a design algorithm for selecting heat exchangers. Jeevan et al. (5) used a genetic algorithm to optimize the thermal resistance of microchannels along with one-dimensional and two-dimensional finite element methods. They showed that using a genetic algorithm for practical microchannel design can be useful. Bionic fractal microchannels were first introduced by Bejan and Errera (6). They presented a strategy for constructing channels using structural theory, where the flow resistance along the path is minimized. Inspired by the fractal pattern of circulatory and respiratory systems in mammals, Chen and Cheng (7) proposed a new design of an H-shaped fractal branching channel network for cooling electronic chips. The novel design has a stronger capacity for heat transfer and needs less pumping power, according to results comparing it to conventional parallel networks. Pence (8) compared two microchannel heat sinks, tree-shaped and H-shaped, under the same conditions. The results showed that the tree-shaped microchannel has 60% less pressure drop and a 30°C lower wall temperature than the other design. In another study, Xu et al. (9) designed four different models of microchannels (parallel, rectangular, spiral, and tree-shaped) and investigated the effect of different

MCHS structures on chilling electronic components. Zaretabar et al. (10) present a simulation of heat transfer in a heatsink on a computer's mainboard transistorized square chip. Xu et al. (11) investigated the heat transfer performance of a fractal microchannel network made of silicon and cooled by water under pulsation flow conditions, both experimentally and numerically. Oyewola et al. (12) present an air-cooled temperature management module using a unique pin-fin heat sink for Li-ion cells. Among different pin-fin geometries, the uniform height heat sink (case 2) stands out, showing superior performance. Alrwashdeh et al. (13) focus on the impact of heat exchanger length on parallel and counterflow HEs. Computer simulations reveal that increasing the HE length improves heat transfer, enhances temperature distribution, and boosts energy transfer efficiency within the HEs. Yan et al. (14) designed an optimal dual-objective thermal-hydraulic model and compared it with optimal hydraulic and optimal thermal models. The results showed that the optimal dual-objective model with 15 main branches has the best overall performance.

In recent years, the use of nanofluids and mixing nanoparticles with base fluids to increase heat transfer has been the subject of much research. Nanofluids are new fluids made from the dispersion of nano-scale materials such as nanoparticles, nanotubes, and nanowires in a base fluid. In other words, nanofluids are suspensions in which solid nanomaterials are added to the base fluid and suspended within the fluid to increase the base fluid's heat transfer properties. Adding nanoscale particles with higher thermal conductivity coefficients to the base fluid is one of the most common techniques to increase heat transfer. The idea of using nanoparticles was first proposed by Maxwell in 1881, which sparked a major change in the study of heat transfer in fluids. Later on, Choi and Eastman (15) used nanofluids to increase heat transfer. Keblinski et al. (16), based on studies of nanofluids, found that thermal conductivity increases with decreasing particle size. They showed that the key factors in comprehending the thermal properties of nanofluids are the nature of the motion path rather than diffusion, heat transfer in nanoparticles, and the direct or mediated effects of fluid clustering that provide pathways for rapid heat transfer. Abu-Nada et al. (17) studied natural heat transfer in circular loops by using nanofluids. They showed that adding different types and different volume fractions of nanoparticles has different effects on heat transfer properties. Pasha and Domiri-Ganji (18) analyzed heat transfer and angular velocity of micropolar ethylene-glycol nanofluid over various fins on a stretching sheet, revealing maximum temperature at the last fin and higher angular velocity for triangular and chamfer fins. Ho and Chen (19) investigated experimentally forced convection heat transfer utilizing an Al_2O_3-water nanofluid in a copper minichannel heat sink. In their study, Hatami and Ganji (20) investigated the heat transfer characteristics of a MCHS with multiple fins. The cooling fluid flow employed in their experiment was a water-copper nanofluid and optimized the heat sink geometry considering the minimum friction coefficient. Jalili et al. (21) evaluate the heat transfer of Al_2O_3-water nanofluid in a heatsink with a magnetic field using the KKL model. Abdollahi et al. (22) investigate the flow and thermal characteristics of a MCHS using a hybrid nanofluid with copper nanoparticles. The results showed the impact of nanoparticle volume fraction and Darcy number on heat transfer and temperature distribution. Jalili et al. (23) looked at how different things affected the temperature, speed, and concentration distribution of a micro-polar nanofluid in a rotating system with parallel plates. Jalili et al. (24) compared the accuracy of three methods using Finite Element, and Runge-Kutta for simulating thermal diffusivity profiles in oblique stenosis arteries by hybrid nanofluids with Al_2O_3 and Cu nanoparticles. The Finite Element method came in second place (with less than 9% error), with Akbari-Ganji method having the highest accuracy (less than 7% error). In another study, Jalili et al. (25) investigate the impact of thermo-diffusion, electrical field, and nonlinear thermal radiation on the flow of a non-Darcy Casson fluid on stretched surfaces using the Hybrid Analytical and Numerical (HAN) Method, considering various parameters and their effects on velocity, temperature, and concentration. In recent study, Jalili et al. (26) examined the flow of a viscous fluid between porous disks under a magnetic field, comparing Akbari-Ganji Method (AGM) and the Finite Element Method (FEM). Valuable research has been conducted in the fields of microchannels, nanofluids, and heat transfer, which are reportd in literature (27-32) and can be beneficial for future studies.

In the present study, fluid flow and heat transfer in a fractal microchannel heat sink have been simulated using the COMSOL Multiphysics software. The use of a fractal structure is motivated by its higher heat transfer capability and lower pumping power compared to a parallel microchannel structure. The fractal microchannel investigated in this research has been proposed by scientists in recent years and features 15 branches, representing the most thermo-hydraulically optimized configuration. Since nanofluids have not been used in this particular geometry before, and considering the need for enhanced heat transfer in heat sinks to prevent chip overheating, three different nanofluids (water-copper, water-Al_2O_3, and water-TiO_2) have been employed as coolant fluids at various volume fractions compared to the base fluid (water). The three nanofluids have been evaluated hydrodynamically and thermally, considering parameters such as pumping power and Nusselt number, and the best nanofluid for overall performance enhancement of the fractal microchannel has been determined. Furthermore, to increase the efficiency of the

microchannel and investigate the effect of geometric modifications inside the fractal microchannel, cavities and fins have been introduced. Both new geometries have been evaluated thermo-hydraulically and compared to the base geometry. Ultimately, a new and optimized geometry has been proposed for future work to further enhance performance.

2. PROBLEM STATEMENT

2. 1. Physical Model In this study, fluid flow and heat transfer in a fractal microchannel heat sink in the presence of three nanofluids will be investigated using numerical simulation. The use of numerical methods allows for the flexibility to modify problem conditions, including boundary conditions and various parameters, based on the physics and geometry of the problem. The microchannel heat sink geometry studied in this research is presented by Yan et al. (14). The fractal microchannels are inspired by the fractal patterns found in mammalian circulatory and respiratory systems, and they exhibit enhanced heat transfer and reduced pumping power compared to other microchannels. The fractal microchannel studied in this research represents an optimized thermo-hydraulic configuration which is shown in Figure 1. It consists of 15 main branches, as depicted in Figure 1, but for computational convergence and improved computational efficiency, a one-fifteenth section of the overall structure, as shown in Figure 2, is considered for numerical simulation. The COMSOL Multiphysics software, known for its capabilities in fluid mechanics, is used for the numerical simulation. Since COMSOL can import geometry from CAD software, the simulation geometry is designed in Solidworks and imported into COMSOL. The studied geometry consists of an inlet in the center and eight outlet branches formed along the radius, as shown in Figure 2. The overall radius of the geometry is 11 millimeters, the inlet branch radius is 1 millimeter, the height of the channel bed is 0.2 millimeters, and the channel height is 0.5 millimeters. Heat flux is applied from the bottom to the heat sink, and the fluid flow inside the microchannel induces heat transfer.

Given the enhanced heat transfer characteristics of nanoparticles, the utilization of nanofluids can improve the performance of microchannel fractal heat sinks. However, this aspect has not been addressed in previous studies. In this research, the aim is to enhance heat transfer using copper (Cu), alumina (Al_2O_3), and titanium dioxide (TiO_2) nanoparticles in water as the base fluid, with nanoparticle volume fractions ranging from 0 to 4%. Various parameters, including temperature distribution, pressure drop, pumping power, and heat sink performance coefficient, have been investigated within an inlet flow rate range of 200 to 400 mil/min and a constant heat flux of 100 W/cm². Finally, a comparison has been made among the three nanofluids.

To enhance the geometric properties, square-shaped fins and cavities have been introduced within the initial three branches of the microchannel fractal. The cross-sectional shape of both the cavities and fins is square, with their respective heights being equal to the height of the microchannel. Six fins or cavities have been produced in each microchannel branch, as depicted in Figure 3.

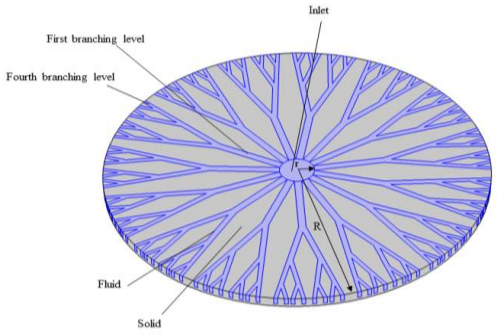

Figure 1. Schematic geometry of MCHS

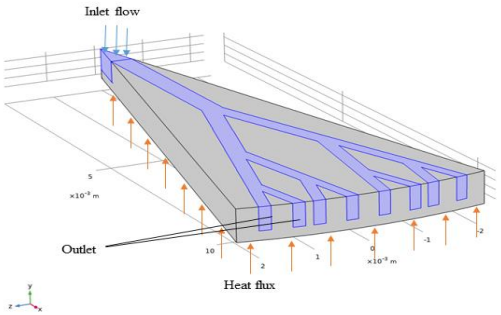

Figure 2. Schematic geometry and boundary conditions

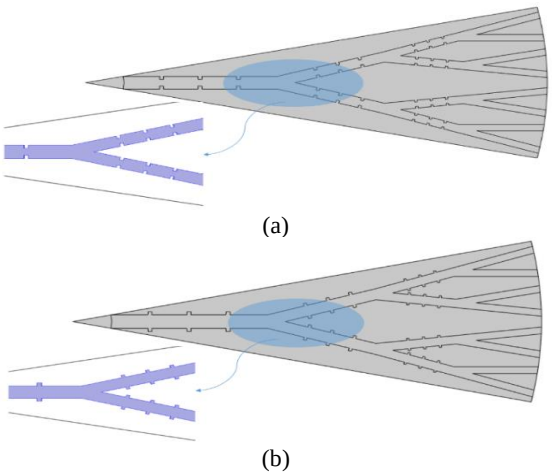

Figure 3. Geometry of microchannel a: with fin b: with cavity

2. 2. Numerical Model The properties of nanofluids have been calculated using the following equations:

The viscosity of nanofluids for spherical nanoparticles can be estimated using the following equation (33):

$$\mu_{nf} = \frac{\mu_f}{(1-\varphi)^{2.5}} \quad (1)$$

The density and specific heat capacity of a nanofluid with any shape of nanoparticle can be obtained from the following equations:

$$\rho_{nf} = \left(\frac{m}{V}\right)_{nf} = (1-\varphi)\rho_f + \varphi\rho_s \quad (2)$$

$$\left(\rho \cdot c_p\right)_{nf} = (1-\varphi)\left(\rho \cdot c_p\right)_f + \varphi\left(\rho \cdot c_p\right)_s \quad (3)$$

The effective thermal conductivity coefficient of a nanofluid can be approximately obtained from the following equation by Hamilton-Crosser model (34):

$$\frac{k_{nf}}{k_f} = \frac{k_s+(n-1)k_f-(n-1)(k_f-k_s)\varphi}{k_s+(n-1)k_f+(k_f-k_s)\varphi} \quad (4)$$

where n is the shape factor of nanoparticles, which for spherical nanoparticles is equal to 3. As a result, only spherical nanoparticles can be used with this equation; other shapes of nanoparticles are not taken into account. The use of this model is suitable for studying the enhancement of heat transfer using appropriate nanoparticles. In the above equations, φ represents the volume fraction of nanoparticles. The thermodynamic properties of the base fluid and nanoparticles are introduced in Table 1.

Fluid behavior in a control volume is described using the Navier-Stokes equations (35), which are expressed as:

Continuity equation: To investigate the conservation of mass, the continuity equation is used in the following form:

$$\nabla \cdot \left(\rho_f \vec{u}\right) = 0 \quad (5)$$

Momentum equation:

$$\vec{u} \cdot \nabla\left(\rho_f \vec{u}\right) = -\nabla p + \nabla \cdot \left(\mu_f \nabla \vec{u}\right) \quad (6)$$

Energy equation for fluid:

$$\vec{u} \cdot \nabla\left(\rho_f c_{p.f} T_f\right) = \nabla \cdot \left(k_f \nabla T_f\right) \quad (7)$$

TABLE 1. Thermodynamic Properties (17)

Thermodynamic properties		ρ (Kg/m³)	c_p (J/KgK)	k (W/mK)
Base fluid	**Water**	997.1	4179	0.613
Nanoparticles	**Cu**	8933	385	401
	Al_2O_3	3970	765	40
	TiO_2	4250	686.2	8.9538

Energy equation for solid:

$$\nabla \cdot (k_s \nabla T_s) = 0 \quad (8)$$

where $\vec{u}$ is the velocity, ρ_f is the coolant fluid density, $\vec{p}$ is the hydrodynamic pressure, μ_f is the viscosity of the fluid, $c_{p.f}$ is the specific heat capacity of the fluid, T_f represents the temperature of the fluid, k_f is the fluid's thermal conductivity coefficient, k_s and T_s respectively represent the thermal conductivity coefficient of the solid and the temperature of the solid section.

The following parameters are used to evaluate the efficacy of a MCHS:

Pumping power:

$$W_{pump} = \Delta P_{tot} \times q_v \quad (9)$$

where ΔP_{tot} represents the total pressure drop and q_v denotes the volumetric flow rate.

Average Re in each branch:

$$Re_{m.i} = \frac{\rho \times u_{m.i} \times D_h}{\mu} \quad (10)$$

Average Nusselt number in each branch:

$$Nu_{m.i} = \frac{q \times D_{h.i}}{k_f \times (T_{m.wi} - T_{m.fi})} \quad (11)$$

where D_h is the hydraulic diameter, q is the heat flux. Additionally, $T_{m.wi}$ and $T_{m.fi}$ represent the average wall temperature and the bulk fluid temperature, respectively.

Friction factor:

$$f = 2\Delta P \frac{D_h}{L} \frac{1}{\rho {u_{in}}^2} \quad (12)$$

performance evaluation criterion:

$$PEC = \frac{\left(\frac{Nu_{ave}}{Nu_{ave.\varphi=0}}\right)}{\left(\frac{f}{f_{\varphi=0}}\right)^{\left(\frac{1}{3}\right)}} \quad (13)$$

2. 3. Boundary Conditions Based on Figure 2, the boundary conditions are determined. In the operating temperature range, the fluid flow is steady, incompressible, and has constant thermophysical properties. The volume fraction of the nanoparticles under investigation in this study is 2% and 4%. The inlet temperature is 293 K, the inlet flow rate is 200 ml/min, and the outlet pressure is equal to atmospheric pressure. The heat sink is made of copper and is isolated from the surrounding environment. The heat flux entering the heatsink's bottom wall is 100 W/cm^2. A no-slip condition is applied to the walls, and the effects of radiation and gravity are neglected.

2. 4. Grid Independence In the numerical solution process in software, one of the most important issues is creating an appropriate grid or mesh. The importance of grid generation in numerical simulation is that if the grid is not fine enough, calculations will not have high

accuracy, and if the grid is too fine, the cost and time of performing the simulation will be significantly high. Therefore, the grid should be fine enough that the results do not differ significantly from each other and are essentially independent of the mesh. In grid generation, it should be noted that the meshes near the walls and edges, where the gradient of flow variables is more intense, should be finer to have a higher accuracy in the calculations. Also, the grid in the solid part can be larger than the liquid part. To evaluate the accuracy of the results, the maximum temperature and pressure drop were investigated in five different grid generations. The numbers of grids 384073, 698638, 903316, 1314415, and 1693388 were studied. Considering the obtained results, the changes in the maximum temperature and pressure drop in the third grid and later are very negligible. Therefore, a mesh number of 903316 has been chosen to continue the process.

2. 5. Validation For validation, the obtained pumping power from the simulation has been compared with the pumping power versus flow rate graph introduced by Yan et al. (14). In this validation, the coolant fluid is water, and the heat flux is 50 W/cm^2. As can be seen in Figure 4, the obtained results have a good agreement with the data in the article.

3. RESULTS AND DISCUSSION

This study seeks to assess the thermal performance of a microchannel heat sink operating under laminar flow conditions. Moreover, endeavors are undertaken to enhance the heat sink's efficiency by introducing nanofluid flow and incorporating fins and cavities within the microchannel. Through a thorough investigation, the optimal nanoparticles and geometry have been identified to improve the thermal-hydraulic performance. The primary objective of employing a heat sink is to mitigate the temperature rise of the electronic chip, with achieving a low maximum heat sink temperature being crucial for this purpose. Maintaining a low maximum temperature ensures improved heat sink performance and prevents chip failure resulting from elevated temperatures. Therefore, the enhancement of system geometry and the utilization of nanoparticles in thermal systems not only guarantee efficiency and improved performance but also contribute to cost reduction and energy consumption.

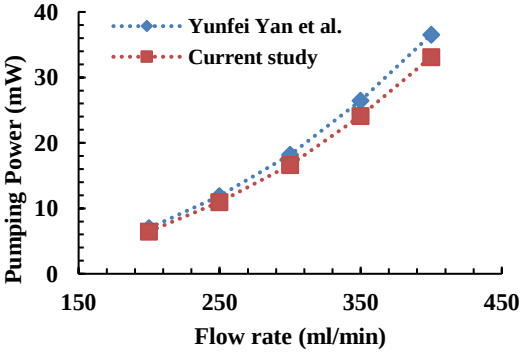

Figure 4. Model validation

3. 1. Applications of Nanofluids Figure 5 illustrates the variations in the maximum temperature of the heatsink in relation to the flow rate for nanofluids: Cu-water, Al_2O_3-water, and TiO_2-water. As observed, as the inlet flow rate and fractional volume of nanoparticles increase from zero to four percent, the maximal temperature of the MCHS decreases. An increase in the inlet flow rate causes an increase in the inlet velocity, which raises the Reynolds number. The temperature differential between the inlet and outlet of the flow is decreased by raising the inlet flow rate while keeping the heat flux constant. As a result, the flow's output temperature drops when the incoming flow temperature is constant. In general, it can be said that when the inlet flow rate rises, the efficiency of heat transfer between the fluid and the wall also increases, which lowers the temperature of the microchannel heat sink. The heat sink's maximum temperature for water flow is 349.28 K at a flow rate of 200 ml/min and 334.1 K at a flow rate of 400 ml/min.

Figure 5 shows the impact of introducing solid nanoparticles at flow rates between 200 and 400 ml/min at volume fractions of 2% and 4% on the heat sink's maximum temperature. The addition of solid nanoparticles improves thermophysical characteristics, such as the thermal conductivity of the coolant fluid and heat transfer, as shown in Figure 5. It is worth mentioning that increasing the inlet flow rate (increasing fluid velocity) and the fractional volume of solid nanoparticles result in a reduction in the temperature gradient along the fluid path. Consequently, the heat sink's maximum temperature is decreased, and its temperature distribution is more uniform.

In Figure 6, contour plots depicting the influence of two parameters, namely volume fraction and inlet flow rate, on temperature are observed. As evident from the plot, an increase in volume fraction and inlet flow rate results in a decrease in the temperature of the heat sink. These plots, which display the variations in temperature profiles, provide valuable insights into the three parameters under discussion. Furthermore, the three-dimensional plot enhances our understanding of the intricate behavior of fluid flow.

In Figure 7, the maximal temperature of the MCHS in the presence of Al_2O_3-water, TiO_2-water, and Cu-water nanofluids at a 4% volume fraction has been compared. As observed, the Cu-water nanofluid has the lowest temperature, followed by Al_2O_3-water and TiO_2-water.

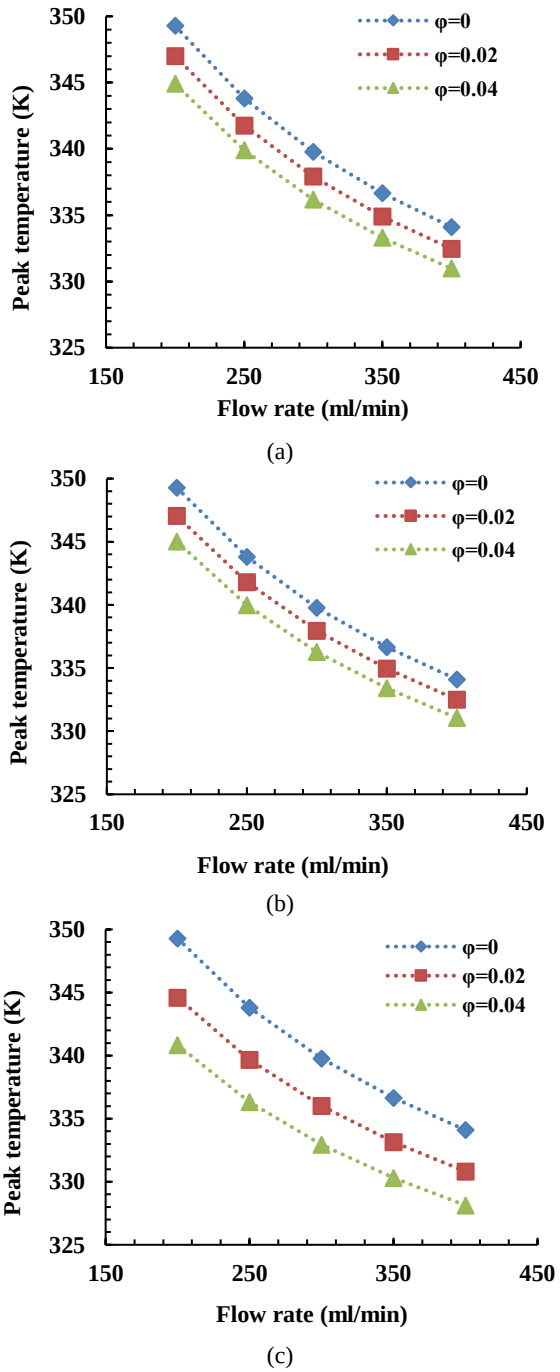

Figure 5. Maximum temperature in the heat sink for (a) Al_2O_3-water, (b) TiO_2-water, and (c) Cu-water

The maximum temperature at a flow rate of 200 ml/min for Cu-water, Al_2O_3-water, and TiO_2-water nanofluids is 340.83, 344.91, and 345.01 K, respectively. The reason for this is the thermal conductivity coefficient, which is higher for water-copper than the other two nanofluids.

Figure 8 depicts the temperature distribution observed when water and three different nanofluids, each with a fractional volume of 4%, are subjected to a flow rate of 200 ml/min. The use of nanoparticles effectively mitigates the temperature gradient, leading to a homogeneous distribution of temperature within the fractal microchannel heat sink. Hot spots can be noticed in certain regions where fluid flow pathways are absent, and these hot spots can be mitigated by employing tree-like structures. The utilization of fractal-based compensatory structures has been employed to mitigate heat transfer degradation and establish regions of enhanced heat transfer. By increasing the number of branches in the fractal tree structure, the temperature

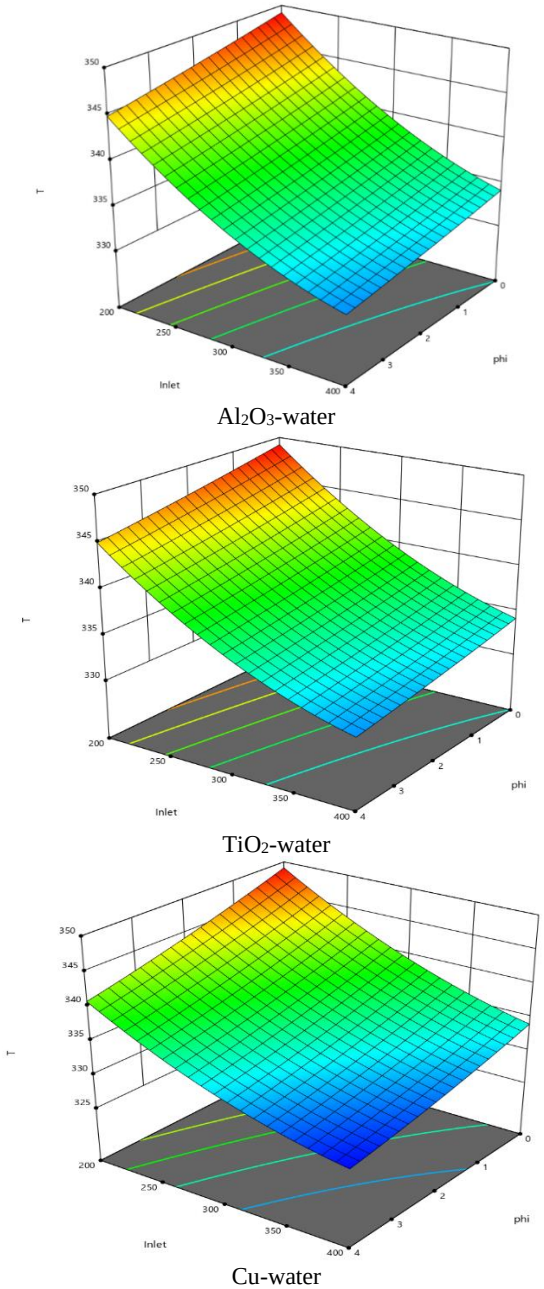

Figure 6. Effects of various operating parameters

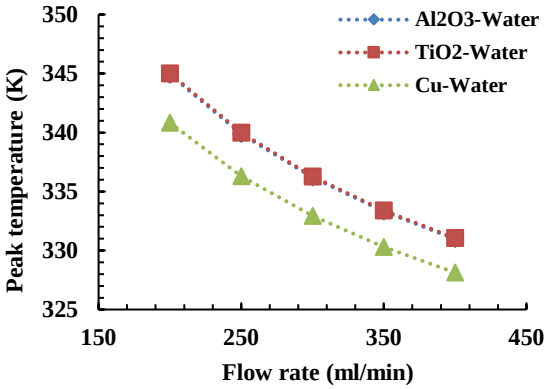

Figure 7. maximum temperature in the heat sink at 4% volume fraction

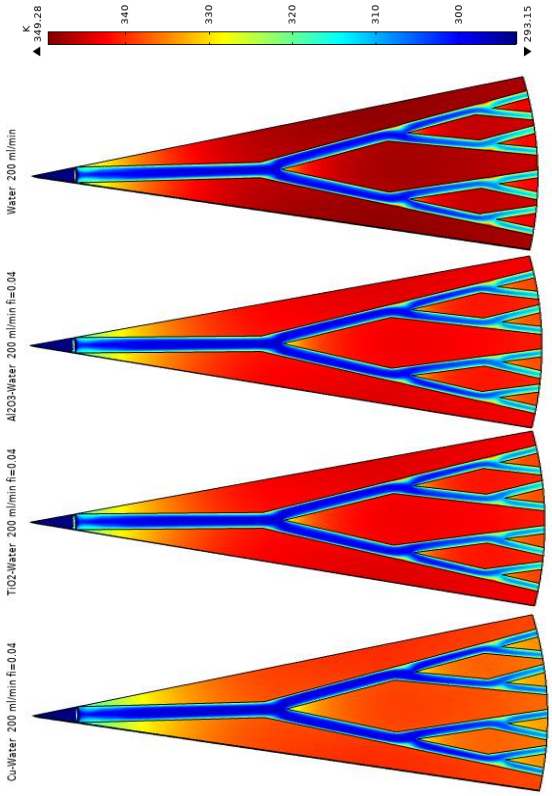

Figure 8. Temperature distribution in heat sink

distribution in these regions becomes more uniform, preventing the formation of abrupt temperature gradients. Furthermore, it can be observed that in the branching regions of the new microchannel configurations, the boundary layer becomes turbulent and redevelops inside the microchannel. This phenomenon leads to enhanced heat transfer in these regions compared to the core of the microchannel. Additionally, it is noticeable that near the walls, lower temperatures are present compared to the regions away from the walls. This is attributed to the increased heat transfer between the wall and the fluid. An increase in the solid volume fractions in nanofluids has been found to significantly enhance several thermophysical parameters, with particular emphasis on the thermal conductivity of the coolant fluid. This phenomenon accelerates the process of thermal energy transmission and guarantees a consistent distribution of temperature throughout the surfaces.

Figure 9 depicts the variations in pumping power as a function of flow rate, considering the fractional volume of the three discussed nanofluids. It should be noted that the pumping power is obtained based on Equation 9. The pumping power is influenced by both geometric parameters and thermophysical variables, including density, dynamic viscosity, and inlet velocity. As observed, the pumping power increases with an increase in the inlet flow.

With the inclusion of nanoparticles, the coolant fluid becomes denser and more viscous, increasing the fractional volume and pumping power of all three nanofluids. As a result of the incorporation of nanoparticles into the base fluid, which increases the density and viscosity of the coolant fluid, more pumping force is required to transport nanofluid through microchannels. A notable observation in Figure 9 is that there is a positive correlation between the fractional volume of nanoparticles, the inlet flow rate, and the rate of increase in pumping power. As seen, the pumping power for various volume fractions differs minimally at low inlet flow rates, but this disparity increases at higher flow rates. At a flow rate of 200 ml/min, the pumping power is 6.04 mW, and at a flow rate of 400 ml/min, it is 32.63 mW.

Figure 10 illustrates three-dimensional plots of the pump power profile, volume fraction profile, and inlet flow rate profile for three different nanofluids. As observed, an increase in the volume fraction and inlet flow rate leads to an increase in pump power. By increasing the volume fraction of nanoparticles in the nanofluid, the density and viscosity of the nanofluid

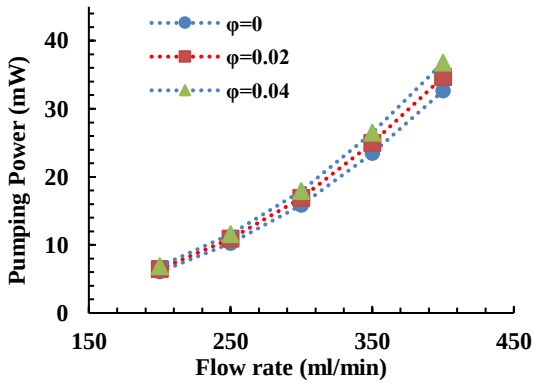

(a)

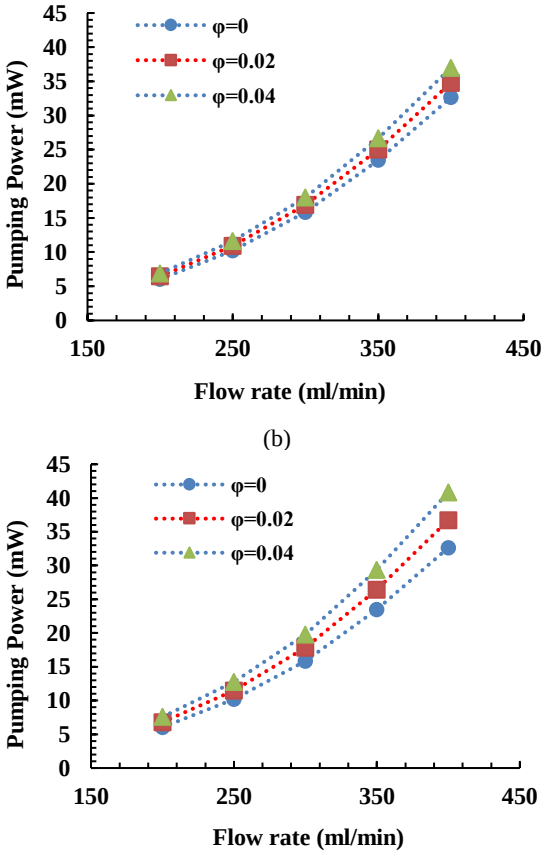

Figure 9. Pumping power for (a) Al_2O_3-water, (b) TiO_2-water, and (c) Cu-water

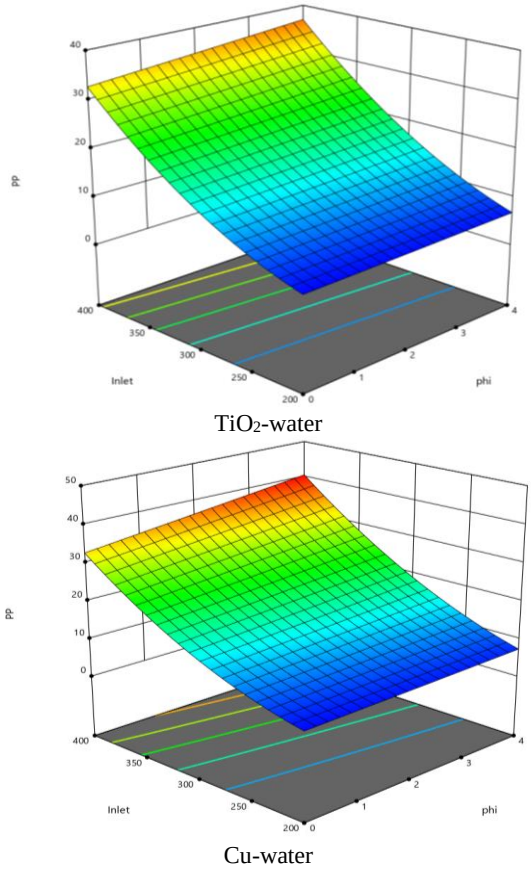

Figure 10. Effects of diverse operating parameters

increase. Moreover, with an increase in the inlet velocity, the collision between the wall and the nanofluid intensifies, further contributing to an increase in density and viscosity. These factors collectively result in an increase in the pumping power required for fluid circulation.

The pressure drop is increased when nanofluids are used in place of water. This is because the nanofluid has a higher viscosity coefficient than water does. In other words, as the base fluid's nanoparticle concentration rises, viscosity rises as well, which in turn raises the pressure drop. The interaction between the additional nanoparticles and the microchannel walls is what caused the increase in viscosity coefficient. Increasing the Reynolds number or flow rate results in a greater velocity gradient, intensifying the collision between nanoparticles and walls, particularly at higher volume fractions. When the inlet flow rate increases, the collision between nanoparticles and microchannel walls becomes more intense, and the force imparted by the walls on the nanoparticles increases, resulting in a higher pressure drop.

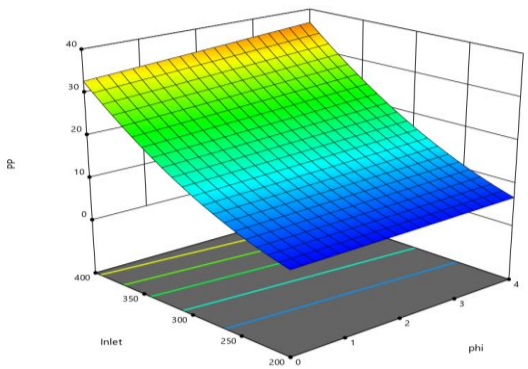

Al_2O_3-water

Figure 11 compares the pumping power of the fractal microchannel in the presence of nanofluids containing 4% volume fractions of Al_2O_3-water, TiO_2-water, and Cu-water. It is evident that the Al_2O_3-water nanofluid exhibits the lowest pumping power, with TiO_2-water and Cu-water nanofluids following in succession. For water-aluminum oxide, water-titanium oxide, and water-copper nanofluids, respectively, the pumping power at a flow rate of 200 ml/min is 6.86, 6.89, and 7.56 mW. The pumping powers of the TiO_2-water and Al_2O_3-water nanofluids are extremely close, with the Al_2O_3-water pumping power being somewhat lower.

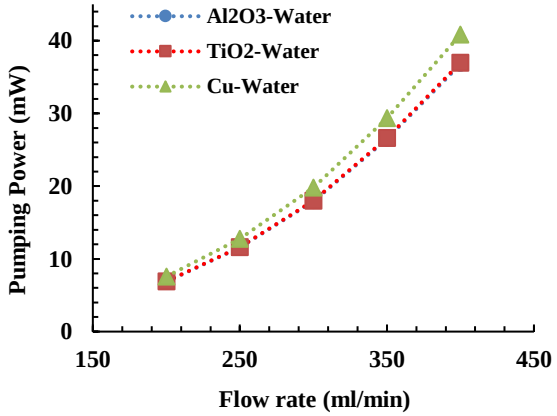

Figure 11. Pumping Power for Nanofluids at a Volume Fraction of 4%

Figure 12 demonstrates that the average Nusselt number varies with the nanoparticle volume fraction at various flow rates. It is significant to remember that the Nusselt numbers differ depending on the volume percentage of the nanoparticles, although the geometric structure of the microchannel and heat flux are the same for all of the scenarios shown in Figure 12. Increasing the inlet flow rate results in a rise in velocity, which improves heat transfer. Due to the reduction in the temperature difference between the wall and the fluid flow, Equation 11 predicts that the Nusselt number will rise. According to Figure 12, the Nusselt number for water is 21.55 for a flow rate of 200 ml/min and 27.51 for a flow rate of 400 ml/min.

The thermal conductivity of the nanofluid increases in comparison to the base fluid by the addition of nanoparticles. As a result, the temperature difference between the nanofluid and the wall is reduced, and the nanofluid and wall exchange more heat. The Nusselt number exhibits rises due to a reduction in the differential temperature across the wall and the nanofluid flow. Copper nanoparticles have led to a greater increase in the Nusselt number than the other two nanoparticles.

In Figure 13, the Nusselt number in a microchannel is compared with a 4% volumetric fraction of water-copper, water-aluminum oxide, and water-titanium oxide. The TiO_2-water nanofluid has the lowest Nusselt number, followed by Al_2O_3-water and water-copper, respectively. The Nusselt numbers at a flow rate of 200 ml/min for TiO_2-water, Al_2O_3-water, and Cu-water nanofluids are 23.49, 23.66, and 25.15, respectively. Al_2O_3-water and TiO_2-water nanofluids have similar Nusselt numbers, with Al_2O_3-water being slightly higher. To consider an idea practical in the study of a subject, it is necessary to examine all aspects of that idea. In the case of thermal performance analysis in microchannels, hydrodynamic parameters must also be considered in addition to thermal parameters. For example, an idea may improve thermal performance but impair the hydrodynamic performance of the flow. Therefore, a parameter must be defined that simultaneously examines both thermal and hydrodynamic performance. In this situation, the Performance Evaluation Criterion (PEC), which considers both the Nusselt number and the friction coefficient, is determined using Equation 13. Figure 14

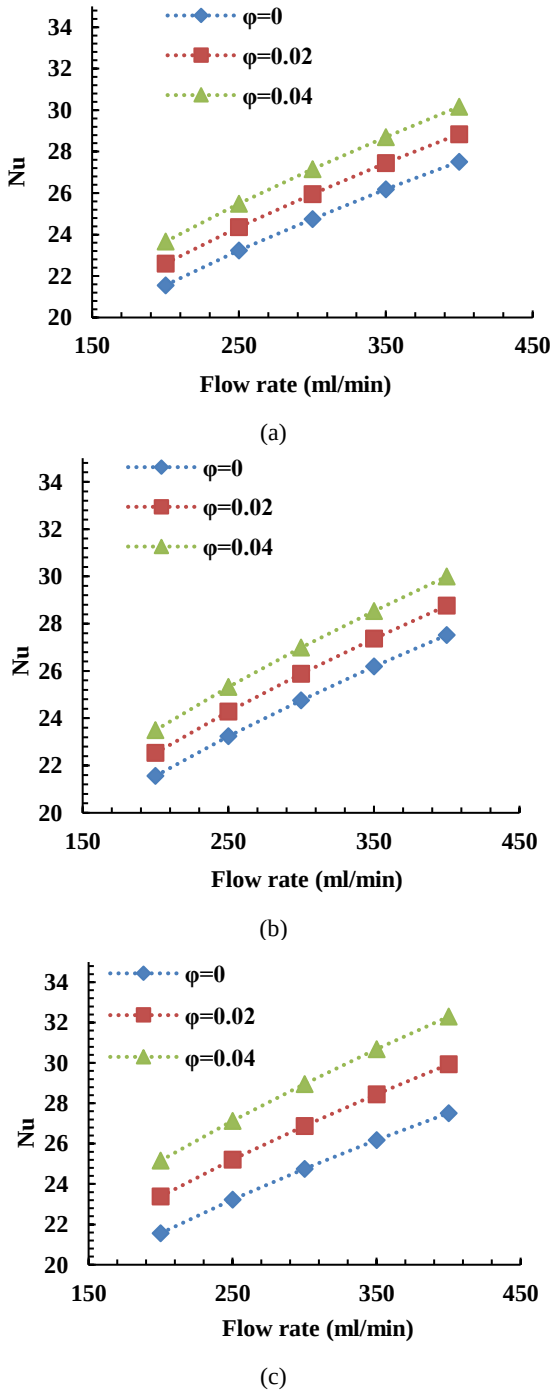

Figure 12. Nusselt Number for (a) Al_2O_3-water, (b) TiO_2-water, and (c) Cu-water

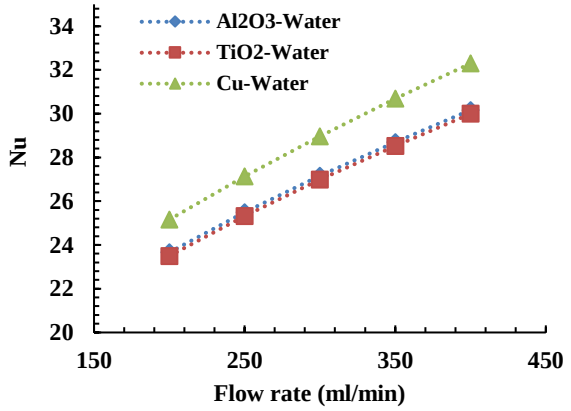

Figure 13. Nusselt Number for Nanofluids at a Volume Fraction of 4 percent

depicts the performance evaluation criteria for the three nanofluids with a 4% volumetric fraction: Al_2O_3-water, TiO_2-water, and Cu-water. The PEC is the ratio of the rise in the Nusselt number to the rise in friction coefficient for each solid volumetric fraction in comparison to the base fluid. Heat transfer and flow fields are influenced by variables such as introducing nanoparticles at various volumetric fractions, fluid velocity, and fluid type. Different things can happen with PEC, depending on how the heat transfer is improved and how much the friction rate goes up. According to Figure 14, each of the three nanofluids has a PEC value above one, demonstrating that the system performs better as a whole when nanoscale particles are added to the base fluid in this configuration. The water-copper nanofluid exhibits the highest PEC. The PEC value is independent of flow rate due to the microchannel shape and laminar flow regime, and only minor changes in the PEC value occur with increasing flow rate.

Based on the above content, it can be concluded that the best overall performance is related to the Cu-water nanofluid, and by adding copper nanoparticles to the water-based fluid, the overall performance of the system can be improved. After Cu-water, the best performance is related to the Al_2O_3-water nanofluid. In the following, to improve the thermal performance of the heat sink, the geometry of the problem will be changed, and the above parameters will be calculated for the new geometries to evaluate the effect of the geometry change as well.

3. 2. Geometry Improvement Figure 15 shows the highest temperature of a heat sink for different inlet mass flow rates for a simple microchannel, a microchannel with cavities, and a microchannel with fins. As observed, as the inlet mass flow rate increases, the maximal temperature of the heat sink decreases. The addition of fins and cavities to the microchannel increases the fluid-solid contact area. This also disturbs the boundary layer, which dissipates and then redevelops. Because of these factors, heat transfer in the new microchannels is better than in the first case, which makes the highest temperature of the heatsink lower. Additionally, the presence of fins in the microchannel boosts flow velocity and causes fluid rotation following the fin, which improves heat transmission and lowers the temperature of the heat sink. The microchannel with fins performs thermally better than the other two microchannels. The presence of cavities and fins in the microchannel leads to the generation of turbulence in the boundary layer and its reformation. This phenomenon, when repeated in the microchannel, enhances heat transfer. Furthermore, increasing the flow rate results in higher heat transfer coefficients and overall heat transfer, leading to a decrease in the overall temperature of the heat sink. The maximum temperature of the heat sink for a flow rate of 200 ml/min is 349.28 for the base microchannel, 345.75 for the microchannel with cavities, and 337.02 K for the microchannel with fins.

Figure 16 depicts the contours of temperature for the three different geometries. Figure 16 shows that the temperature distribution is better and more uniform in the

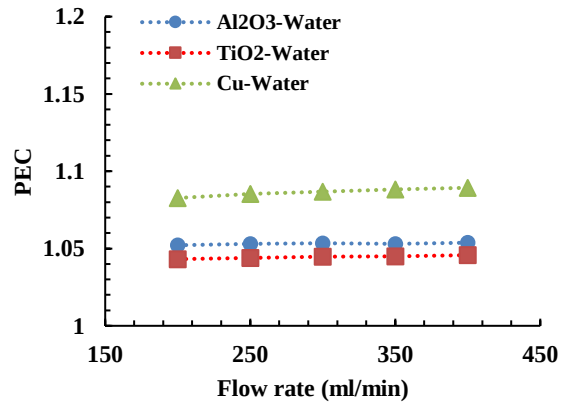

Figure 14. PEC for Nanofluids

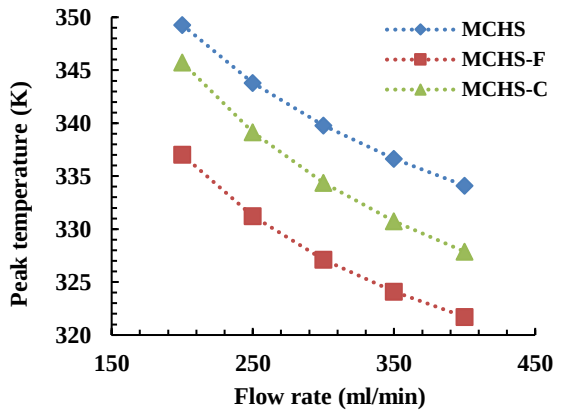

Figure 15. Maximum temperature of the heat sink for three geometries

microchannel with fins (MCHS-F). Additionally, it is evident from Figure 16 that the simple microchannel's maximum temperature is located in the geometry's center, specifically near the second and third branches. However, for the two new geometries, the highest temperature is around the radius of the geometry and the fourth branch. The minimum temperature is located at the center of the microchannel and increases along the microchannel walls. Additionally, the effects of branching and the addition of cavities and fins are noticeable, leading to turbulence in the boundary layer. In cavities, the boundary layer becomes turbulent and then redevelops. Furthermore, the presence of cavities creates stagnant regions and increases the fluid-wall contact area, which results in enhanced heat transfer. In microchannels with fins, in addition to these factors, the fluid velocity experiences a sudden increase at the locations where fins are present, leading to further enhancement of heat transfer.

Figure 17 shows how the pumping power changes when the flow rate changes for a basic microchannel, a microchannel with a cavity (MCHS-C), and a microchannel with a fin (MCHS-F). Notably, Equation 9 is used to determine the pumping power. As can be seen, the pumping power rises as the flow rate rises. Following the formation of cavities or fins, the branches produce a reverse pressure gradient, increasing the overall pressure drop. The cavity and fin cause turbulence in the fluid flow, which causes low-pressure and high-pressure areas

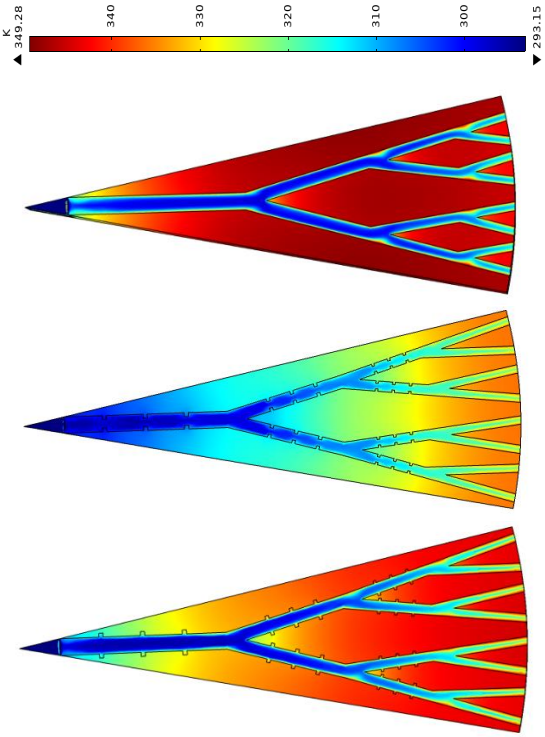

Figure 16. Temperature distribution in heat sink

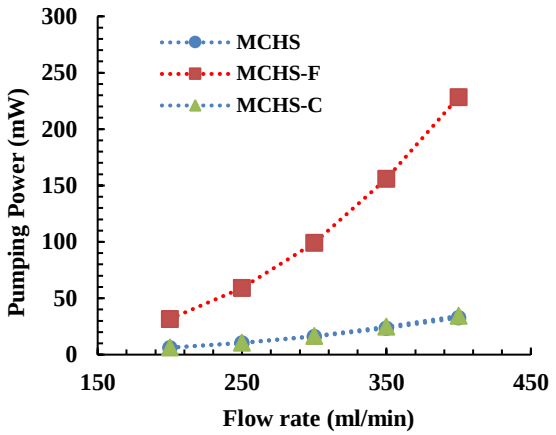

Figure 17. Pumping power for three geometries

to occur all around them. Consequently, the non-uniform distribution of pressure leads to an overall increase in the magnitude of the pressure drop. By adding cavities and fins, the boundary layer becomes turbulent, and the presence of cavity and fin walls creates local flow patterns in different paths, leading to increased pressure drop and pump power consumption. Based on Figure 17, it is clear that adding fins significantly reduces the pressure drop as compared to the cavity, and this difference is larger as the inlet flow rate rises.

Figure 18 shows a comparison of the Nusselt number in three different geometries. The microchannel with the fin has the highest Nusselt number, indicating greater heat transfer and a smaller temperature difference between the microchannel wall and bulk fluid. The reason for this increase is the higher fluid velocity in the microchannel with fins, which leads to enhanced heat transfer between the channel walls and the fluid. As a result, the temperature difference between the microchannel walls and the bulk fluid temperature decreases. The Nusselt number for a simple

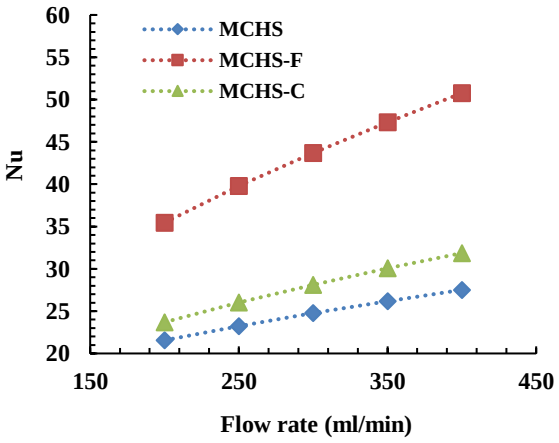

Figure 18. Nusselt number for three geometries

microchannel at an inlet flow rate of 200 mil/min is 21.55, while for a microchannel with cavities and a microchannel with fins, it is 23.69 and 35.45, respectively.

The microchannel with fins (MCHS-F) has greater heat transfer performance, but it also has a higher pressure drop and pumping power compared to the other two geometries, according to the information presented. The Performance Evaluation Criteria (PEC) was investigated in order to thoroughly study the pressure drop and heat transfer characteristics, as illustrated in Figure 19. As can be observed, the mass flow rate increases with all PEC values, suggesting that greater mass flow rates (higher velocities) are advantageous for enhancing heat sinks' general performance. With an increase in mass flow rate and flow velocity, heat transfer is enhanced, and the impact of viscous forces is diminished. Figure 19 reveals that the PEC value for the MCHS-F microchannel is lower than that of the microchannel without fins, indicating that fins reduce the overall system performance. The microchannel with cavities exhibits a PEC value greater than one, suggesting an enhancement in the overall performance of the system.

Based on the parameters discussed above, it can be concluded that the microchannel with cavities exhibits better overall performance compared to the other two microchannels. The geometry of the microchannel with cavity can be a suitable option for heat dissipation in electronic chips and significantly reduces the temperature of the heat sink.

In Figure 20, the results of geometry modification and cavity creation are compared with the results presented in Yan et al.'s paper (36). They utilized a double-layered microchannel heat sink in their study and investigated various parameters. The baseline geometry of both heat sinks is the same, and a new geometry is proposed in both studies. The performance evaluation coefficient is the parameter discussed in both papers. As evident from the figure, at flow rates ranging from 200 to400 mil/min,

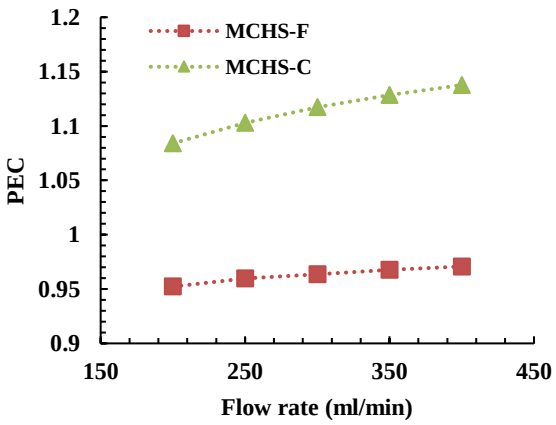

Figure 19. PEC for two new geometries

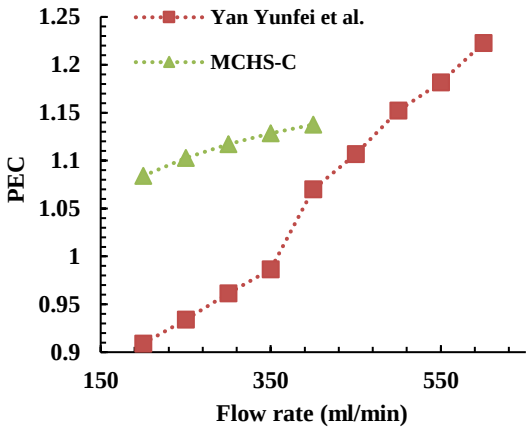

Figure 20. Comparison of Results with Yunfei's Paper

the proposed geometry in the current paper (microchannel with cavity) exhibited better overall performance and could be beneficial for future applications. However, with an increase in flow rate, the geometry proposed by Yan et al. [36] showed a significant improvement in performance, and at high flow rates, using that geometry could be advantageous.

4. CONCLUSIONS

This study utilized the COMSOL Multiphysics software, incorporating heat transfer in solids and fluids along with laminar flow physics in three dimensions. The investigation specifically delved into the characteristics of fluid flow when employing nanofluids, including water-copper, water-aluminum oxide, and water-titanium oxide, at various volume fractions and flow rates ranging from 200 to 400 ml/min. Following these analyses, modifications were made to the geometry of the problem to enhance the heat sink's performance, involving the introduction of fins and cavities within the microchannel. To comprehensively assess the thermal and hydraulic performance of the microchannel, the performance evaluation criterion was calculated to identify the optimal case from both thermal and hydraulic perspectives. A detailed summary of the results will be presented in the subsequent analysis.

4. 1. Examination of the Results of Nanofluid Utilization:

- Initially, the results showed that using nanofluids increases heat transfer and improves thermal conditions, which is due to the increased heat transfer coefficient. The maximum heatsink temperature for the Al_2O_3-water nanofluid at a flow rate of 200 ml/min and a 4% volume fraction decreased by 1.25% compared to water. This value

was 1.22% for TiO_2-water and 2.41% for Cu-water. According to the results, the Cu-water nanofluid has the highest increase in heat transfer and the lowest maximum temperature.

- Although using nanofluids can increase heat transfer, it also increases pressure drop and, consequently, increases pumping power. However, the increase in the heat transfer coefficient has a significant impact on reducing the maximum temperature, and it is better to bear the cost if needed to compensate for the pressure drop. The pressure drops for the Al_2O_3-water nanofluid at a flow rate of 200 ml/min and a 4% volume fraction increased by 13% compared to water. This value was 14% for TiO_2-water and 25% for Cu-water. Therefore, the pressure drop for the Cu-water nanofluid is higher than the other two nanofluids.
- The examination of the Nusselt number reveals an increase in heat transfer enhancement when using nanofluids. The Nusselt number shows an ascending trend with an increase in volume fraction and flow rate. The average Nusselt number for the Al_2O_3-water nanofluid at a flow rate of 200 ml/min and a volume fraction of 4% increased by 9% compared to water. For the TiO_2-water nanofluid, the increase was 8%, and for the Cu-water nanofluid, it was 16%. Therefore, the average Nusselt number for the Cu-water nanofluid is higher than the other two nanofluids.
- The analysis of the PEC number indicates that all three nanofluids increase the performance coefficient of the heatsink, and at a volume fraction of 4%, this increase is 5, 4, and 8 percent for Al_2O_3-water, TiO_2-water, and Cu-water, respectively. Considering the results, the Cu-water nanofluid has the best overall performance and can be the best option for improving the thermal-hydraulic performance in heat sinks.

4. 2. Examination of the Results of Geometric Changes:

- The microchannel with fins and cavities increases the fluid-solid contact area. This also affects the boundary layer, which breaks up and then forms again. Additionally, the use of fins within the microchannel enhances the velocity of flow. Due to these considerations, heat transfer in the new microchannels is superior to that of the original case, resulting in a lower maximum temperature of the heatsink. The maximum temperature reduction at the heat sink in the microchannel with fins, at a flow rate of 200 ml/min, is 3.5% compared to the initial configuration. For the microchannel with a cavity, this reduction is 1%.
- Although the microchannel with fin provides a more uniform temperature distribution, its pressure drop is much higher than the other two geometries. The pumping power of the flow in the microchannel with fins at a flow rate of 200 ml/min increases by 400% compared to the initial state, while this value is 4% for the microchannel with cavities. Also, with an increasing flow rate, the rate of increase in pressure drop and pumping power of the microchannel with fins is higher.
- Considering the two parameters of heat transfer and pressure drop, the microchannel with cavities performs better, and the performance of the microchannel with fins is lower than the base microchannel. The overall system performance drops by 4% when using a microchannel with fins, and if a microchannel with cavities is used, the performance improves by 8%.

5. REFERENCES

1. Agostini B, Fabbri M, Park JE, Wojtan L, Thome JR, Michel B. State of the art of high heat flux cooling technologies. Heat transfer engineering. 2007;28(4):258-81. https://doi.org/10.1080/01457630601117799
2. Wang G, Qian N, Ding G. Heat transfer enhancement in microchannel heat sink with bidirectional rib. International Journal of Heat and Mass Transfer. 2019;136:597-609. https://doi.org/10.1016/j.ijheatmasstransfer.2019.02.018
3. Tuckerman DB, Pease RFW. High-performance heat sinking for VLSI. IEEE Electron device letters. 1981;2(5):126-9. https://doi.org/10.1109/EDL.1981.25367
4. Weisberg A, Bau HH, Zemel J. Analysis of microchannels for integrated cooling. International Journal of Heat and Mass Transfer. 1992;35(10):2465-74. https://doi.org/10.1016/0017-9310(92)90089-B
5. Jeevan K, Quadir G, Seetharamu K, Azid I, Zainal Z. Optimization of thermal resistance of stacked micro-channel using genetic algorithms. International Journal of Numerical Methods for Heat & Fluid Flow. 2005;15(1):27-42. https://doi.org/10.1108/09615530510571930
6. Bejan A, Errera MR. Deterministic tree networks for fluid flow: geometry for minimal flow resistance between a volume and one point. Fractals. 1997;5(04):685-95. https://doi.org/10.1142/S0218348X97000553
7. Chen Y, Cheng P. Heat transfer and pressure drop in fractal tree-like microchannel nets. International Journal of Heat and Mass Transfer. 2002;45(13):2643-8. https://doi.org/10.1016/S0017-9310(02)00013-3
8. Pence D. Reduced pumping power and wall temperature in microchannel heat sinks with fractal-like branching channel networks. Microscale Thermophysical Engineering. 2003;6(4):319-30. https://doi.org/10.1080/10893950290098359
9. Xu S, Hu G, Qin J, Yang Y. A numerica1 study of fluid flow and heat transfer in different microchannel heat sinks for electronic chip cooling. Journal of mechanical science and technology. 2012;26:1257-63. https://doi.org/10.1007/s12206-012-0209-x
10. Zaretabar M, Asadian H, Ganji D. Numerical simulation of heat sink cooling in the mainboard chip of a computer with temperature dependent thermal conductivity. Applied Thermal Engineering. 2018;130:1450-9. https://doi.org/10.1016/j.applthermaleng.2017.10.127

11. Xu S, Wang W, Fang K, Wong C-N. Heat transfer performance of a fractal silicon microchannel heat sink subjected to pulsation flow. International Journal of Heat and Mass Transfer. 2015;81:33-40. https://doi.org/10.1016/j.ijheatmasstransfer.2014.10.002
12. Oyewola OM, Awonusi AA, Ismail OS. Performance improvement of air-cooled battery thermal management system using sink of different pin-fin shapes. Emerging Science Journal. 2022;6(4):851-65. https://doi.org/10.28991/ESJ-2022-06-04-013
13. Alrwashdeh SS, Ammari H, Madanat MA, Al-Falahat AaM. The effect of heat exchanger design on heat transfer rate and temperature distribution. Emerging Science Journal. 2022;6(1):128-37. https://doi.org/10.28991/ESJ-2022-06-01-010
14. Yan Y, Yan H, Yin S, Zhang L, Li L. Single/multi-objective optimizations on hydraulic and thermal management in micro-channel heat sink with bionic Y-shaped fractal network by genetic algorithm coupled with numerical simulation. International Journal of Heat and Mass Transfer. 2019;129:468-79. https://doi.org/10.1016/j.ijheatmasstransfer.2018.09.120
15. Choi SU, Eastman JA. Enhancing thermal conductivity of fluids with nanoparticles. Argonne National Lab.(ANL), Argonne, IL (United States); 1995. https://www.osti.gov/biblio/19652
16. Keblinski P, Phillpot S, Choi S, Eastman J. Mechanisms of heat flow in suspensions of nano-sized particles (nanofluids). International journal of heat and mass transfer. 2002;45(4):855-63. https://doi.org/10.1016/S0017-9310(01)00175-2
17. Abu-Nada E, Masoud Z, Hijazi A. Natural convection heat transfer enhancement in horizontal concentric annuli using nanofluids. International Communications in Heat and Mass Transfer. 2008;35(5):657-65. https://doi.org/10.1016/j.icheatmasstransfer.2007.11.004
18. Pasha P, Domiri-Ganji D. Hybrid analysis of micropolar ethylene-glycol nanofluid on stretching surface mounted triangular, rectangular and chamfer fins by FEM strategy and optimization with RSM method. International Journal of Engineering. 2022;35(5):845-54. https://doi.org/10.5829/ije.2022.35.05b.01
19. Ho C-J, Chen W. An experimental study on thermal performance of Al2O3/water nanofluid in a minichannel heat sink. Applied Thermal Engineering. 2013;50(1):516-22. https://doi.org/10.1016/j.applthermaleng.2012.07.037
20. Hatami M, Ganji D. Thermal and flow analysis of microchannel heat sink (MCHS) cooled by Cu–water nanofluid using porous media approach and least square method. Energy Conversion and management. 2014;78:347-58. https://doi.org/10.1016/j.enconman.2013.10.063
21. Jalili B, Rezaeian A, Jalili P, Ommi F, Ganji DD. Numerical modeling of magnetic field impact on the thermal behavior of a microchannel heat sink. Case Studies in Thermal Engineering. 2023;45:102944. https://doi.org/10.1016/j.csite.2023.102944
22. Abdollahi S, Jalili P, Jalili B, Nourozpour H, Safari Y, Pasha P, et al. Computer simulation of Cu: AlOOH/water in a microchannel heat sink using a porous media technique and solved by numerical analysis AGM and FEM. Theoretical and Applied Mechanics Letters. 2023;13(3):100432. https://doi.org/10.1016/j.taml.2023.100432
23. Jalili P, Narimisa H, Jalili B, Ganji D. Micro-polar nanofluid in the presence of thermophoresis, hall currents, and Brownian motion in a rotating system. Modern Physics Letters B. 2023;37(01):2250197. https://doi.org/10.1142/S0217984922501974
24. Jalili P, Sadeghi Ghahare A, Jalili B, Domiri Ganji D. Analytical and numerical investigation of thermal distribution for hybrid nanofluid through an oblique artery with mild stenosis. SN Applied Sciences. 2023;5(4):95. https://doi.org/10.1007/s42452-023-05312-z
25. Jalili P, Azar AA, Jalili B, Ganji DD. Study of nonlinear radiative heat transfer with magnetic field for non-Newtonian Casson fluid flow in a porous medium. Results in Physics. 2023;48:106371. https://doi.org/10.1016/j.rinp.2023.106371
26. Jalili B, Roshani H, Jalili P, Jalili M, Pasha P, Ganji DD. The magnetohydrodynamic flow of viscous fluid and heat transfer examination between permeable disks by AGM and FEM. Case Studies in Thermal Engineering. 2023;45:102961. https://doi.org/10.1016/j.csite.2023.102961
27. Jalili P, D Afifi M, Jalili B, Mirzaei A, D Ganji D. Numerical Study and Comparison of Two-dimensional Ferrofluid Flow in Semi-porous Channel under Magnetic Field. International Journal of Engineering, Transactions B: Applications. 2023;36(11):2087-101. https://doi.org/10.5829/ije.2023.36.11b.13
28. Alibeigi M, Farahani S. Effect of porous medium positioning on heat transfer of micro-channel with jet. International Journal of Engineering. 2020;33(10):2057-64. https://doi.org/10.5829/ije.2020.33.10a.24
29. Vatani M, Domiri-Ganji D. Experimental examination of gas-liquid two-phase flow patterns in an inclined rectangular channel with 90 bend for various vertical lengths. International Journal of Engineering. 2022;35(4):685-91.
30. Ranjbar A, Ramiar A. The effect of viscous dissipation and variable properties on nanofluids flow in two dimensional microchannels. International Journal of Engineering, Transactions A: Basics. 2011;24(2):131-42. https://doi.org/10.5829/ije.2022.35.04A.07
31. Tayari E, Torkzadeh L, Domiri Ganji D, Nouri K. Analytical solution of electromagnetic force on nanofluid flow with brownian motion effects between parallel disks. International Journal of Engineering, Transactions B: Applications. 2022;35(8):1651-61. https://doi.org/10.5829/ije.2022.35.08b.21
32. Tarrad AH. 3d numerical modeling to evaluate the thermal performance of single and double u-tube ground-coupled heat pump. HighTech and Innovation Journal. 2022;3(2):115-29. https://doi.org/10.28991/HIJ-2022-03-02-01
33. Brinkman HC. The viscosity of concentrated suspensions and solutions. The Journal of chemical physics. 1952;20(4):571. https://doi.org/10.1063/1.1700493
34. Hamilton RL, Crosser O. Thermal conductivity of heterogeneous two-component systems. Industrial & Engineering chemistry fundamentals. 1962;1(3):187-91. https://doi.org/10.1021/i160003a005
35. Zamani M, Shafaghat R, Alizadeh Kharkeshi B. Numerical Study of the Hydrodynamic Behavior of an Archimedes Screw Turbine by Experimental Data in order to Optimize Turbine Performance: The Genetic Algorithm. Journal of Applied and Computational Mechanics. 2023. https://doi.org/10.22055/jacm.2023.43137.4031
36. Yan Y, Yan H, Feng S, Li L. Thermal-hydraulic performances and synergy effect between heat and flow distribution in a truncated doubled-layered heat sink with Y-shaped fractal network. International Journal of Heat and Mass Transfer. 2019;142:118337. https://doi.org/10.1016/j.ijheatmasstransfer.2019.06.093

Persian Abstract

چکیده

استفاده از سینک حرارتی میکروکانال یکی از مطمئن‌ترین راه‌حل‌ها برای دفع گرمای تولید شده در تراشه‌های الکترونیکی است. در این مطالعه عددی یک سیک حرارتی میکروکانال فرکتالی مورد بررسی قرار گرفته و از سه نانوسیال آب–مس، آب–اکسید آلومینیوم و آب–اکسید تیتانیوم در کسر حجمی متغیر ۲ و ٤ درصد به عنوان سیال خنک کننده درون میکروکانال استفاده شده است. جریان سیال درون میکروکانال از جهت هیدرودینامیکی و حرارتی مورد بررسی قرار گرفت و پارامترهایی مانند توان پمپاژ، عدد ناسلت و ضریب ارزیابی عملکرد بدست آمد. با توجه به نتایج با افزایش دبی جریان و کسر حجمی نانوذرات انتقال حرارت افزایش پیدا می‌کند. نتایج نشان دادند که حداکثر دمای سینک حرارتی برای نانوسیال آب–مس در دبی ۲۰۰ میلی‌لیتر بر دقیقه و کسر حجمی ٤ درصد، نسبت به آب خالص ۲/٤۱ درصد کاهش داشته‌است که بیشترین مقدار بین نانوسیال‌های دیگر است. ولی از طرف دیگر بیشترین مقدار افت فشار نیز متعلق به نانوسیال آب–مس با مقدار ۲۵ درصد در کسر حجمی ٤ درصد است. با بررسی عدد ضریب ارزیابی عملکرد، مشخص شد که عملکرد هر سه میکروکانال افزایش پیدا می‌کند و نانوسیال آب–مس بهترین عملکرد جامع را دارد که عملکرد کلی را ۸ درصد افزایش می‌دهد و بعد از نانوسیال های آب–اکسید آلومینیوم و آب–اکسید تیتانیوم قرار دارند که به ترتیب ۵ و ٤ درصد عملکرد سیستم را افزایش می دهند. در ادامه برای بهبود عملکرد میکروکانال با هدف افزایش انتقال حرارت و عملکرد کلی سینک حرارتی، فین و حفره‌هایی در سه شاخه اولیه میکروکانال ایجاد شده است. نتایج نشان از افزایش انتقال حرارت برای هر دو هندسه جدید را دارد. حداکثر دمای سینک حرارتی برای میکروکانال با دنده در دبی ۲۰۰ میلی‌لیتر بر دقیقه، نسبت به هندسه اولیه ۳/۵ درصد کاهش داشته‌است که این مقدار برای میکروکانال با حفره ۱ درصد است. با این حال، افت فشار برای میکروکانال با دنده ٤۰۰ درصد بیشتر از هندسه اولیه است که این مقدار برای میکروکانال با حفره ٤ درصد می‌باشد. بررسی عدد ضریب ارزیابی عملکرد نشان داد که استفاده از میکروکانال با حفره عملکرد سیستم را ۸ درصد بهبود می‌بخشد و میکروکانال با دنده عملکرد سیستم را ٤ درصد کاهش می‌دهد.